IEEE Access
Multidisciplinary | Rapid Review | Open Access Journal

Received September 22, 2019, accepted October 6, 2019, date of publication October 17, 2019,
date of current version November 26, 2019.

Digital Object Identifier 10.1109/ACCESS.2019.2948124

Rapid and Precise Reverse Engineering of Complex Geometry Through Multi-Sensor Data Fusion

ZHIQIANG YU[1], TAIYONG WANG[1,2], PENG WANG[1], (Member, IEEE), YING TIAN[1], AND HONGBIN LI[1]

[1]Key Laboratory of Mechanism Theory and Equipment Design of Ministry of Education, Tianjin University, Tianjin 300350, China
[2]Renai College, Tianjin University, Tianjin 301636, China

Corresponding author: Peng Wang (pengwang@tju.edu.cn)

This work was supported in part by the National Natural Science Foundation of China under Grant 51975402, and in part by the Key Laboratory of Mechanism Theory and Equipment Design of Ministry of Education Open Fund.

ABSTRACT This paper presents an effective multi-sensor approach for improving the accuracy of laser scanner by using a tactile probe to perform rapid and accurate reverse engineering of complex objects. The proposed system is unique in that it includes not only the physical integration of the two digitizers but also their combination at the measurement information level. With the coordinate data acquired using the optical scanner, intelligent data segmentation and feature recognition algorithm are proposed to divide the original point set into geometric elements and free-form surfaces. The tactile probe is guided to re-measure each feature with a small number of sampling points. Then different data fusion algorithms are proposed to compensate the scanned data patches of geometric features and free-form features with the accurate tactile probing data. Finally, the compensated point data can be exploited for accurate reverse engineering of a CAD model. Through the fusion of different sensor's information, both sensors complement each other with their advantages. Experimental results show that for the measurement of geometric surface, the proposed method can improve the accuracy of optical measurement to the accuracy of contact measurement. For free-form surface measurement, the proposed method reduces the optical measurement error from +0.032/-0.019 mm to ±0.016 mm, and the standard deviation from 0.012 mm to 0.004 mm. The measurement efficiency of proposed method is 4.5 times higher than that of contact measurement alone.

INDEX TERMS Multi-sensor, reverse engineering, tactile probe, optical scanner, data fusion.

I. INTRODUCTION

Reverse engineering is the process of creating a CAD model from an existing physical part [1]. It has emerged as a crucial methodology to perform rapid product innovative design, especially for complex geometrical shapes [2]. The typical process of reverse engineering begins with 3D data collection through contact or non-contact digitizers. Today, there are various sensors available for 3D data acquisition; however, it has been shown that each technique has its own characteristics and limitations, which lend them to particular applications [3]. Tactile probes are able to provide accurate and reliable measurement, but it is not suitable for the digitization of complex free-form surfaces owing to its inherent slow speed. On the other hand, several non-contact sensors have been developed recently, such as laser beam scanner [4]–[6], structured-light sensors [7]–[9] and stereo vision sensors [10], [11]. These sensors are much more efficient in terms of speed and reduce the human labor required. But the level of measurement accuracy of non-contact digitizers is generally lower than that of contact digitizers.

With the development of modern industry, the single sensor cannot meet the increasing demands on accuracy, efficiency, and complexity of dimensional metrology any more. Therefore, a great deal of multi-sensor measurement systems combining different sensors are developed and implemented to achieve both holistic geometrical measurement and improved reliability of measured data.

The existing multi-sensor system in metrology can be generally divided into the complementary, competitive and

The associate editor coordinating the review of this manuscript and approving it for publication was Porfirio Tramontana.

cooperative system according to sensor configuration [12]. The most common integration pattern is the cooperation of multi-sensors. Chan *et al.* [13] developed a hybrid inspection system by combining coordinate measuring machine (CMM) and stereo-vision system. The spatial location of part on CMM bed is determined by stereo-vision system, and the position information is then used to guide the CMM to achieve the automatic inspection of the measured part. Carbone *et al.* [14] designed a hybrid contact-optical inspection system in which the digitization of the overall object surface is performed using vision system; intelligent feature recognition algorithms are applied to extract the global surface information of the object. The obtained information can be subsequently used to automatically guide the touch trigger probe for precision sampling of critical surface area. A hybrid contact–optical coordinate measuring system is designed by Sładek *et al.* [15], [16], in which the measurement process starts from fast optical data acquisition by a structured light system, and then, numerical analysis is performed to calculate a set of surface points that should be finally re-measured by the CMM. Lu and Wang [17], [18] proposed a multi-sensor approach characterized by the integrated use of a contact scanning probe and a point laser probe. The point laser probe is used to acquire information of the next measuring path of contact scanning probe as it is performing digitization task. With the prior path information from point laser probe, the next scanning path for contact scanning probe is determined real-timely with measurement path planning algorithms. The planned path is subsequently used to guide the contact scanning probe for fast and precise digitization of complex surfaces.

In the above cooperative multi-sensor systems, vision sensor is used only to acquire the part global information such as features positions, and then the probe is guided to make actual measurements to features. Repeated measurements of the whole surface make the system inefficient.

Bradley and Chan [19] presented a complementary sensor metrology approach in which a laser scanner is used to digitize all the free-form surface patches and a touch trigger probe is used to digitize surface patch boundaries. A multi-probe system integrated with a CMM, a structured light sensor, a trigger probe, and a rotary table is introduced by Zexiao *et al.* [20]. The structured light sensor is applied to scan the profile of a part in different views, while the trigger probe is used to measure the edge and key features. Zhao *et al.* [21] proposed an inspection planning strategy that can create inspection plans automatically for the combination of laser scanner and tactile probe in CMM. A knowledge-based method is developed to select the suited sensor for each inspection feature, and the measurement strategies can be automatically planned by the developed inspection planning modules. Mu *et al.* [22] proposed a laser scanner-tactile probe based multi-sensor on machine inspection approach for free-form surface. Point cloud of free-form surface is obtained by laser scanner and machining error is computed at every point. Area out of tolerance can be determined through error contour map method. Finally, extended morphology skeleton algorithm is applied to generate a resample path, along which the tactile probe carries out higher accuracy inspection on the resample zone. Mohib *et al.* [23] introduce a feature-based hybrid inspection planning method, in which feature sequence and sensor selection are addressed. Liu *et al.* [24] proposed a data fusion method for the multi-sensor integrated measuring system, in which the surface data which cannot meet the accuracy requirement of optical scanning are replaced by high precision measurement data from CMM.

The above complementary multi-sensor systems digitize all the surface patches with vision sensor firstly, and the tactile probe is then used to digitize surface patch boundaries and key features. Data from different sensors are simply unified in the same coordinate system as the final digitization result. The measurement accuracy of the system is still limited because the low accuracy data from the non-contact measurement account for the overwhelming majority of the measurement results.

Only limited research on the competitive integration of hybrid contact-optical sensors has been found. Huang and Qian [25], [26] developed a dynamic sensing and modeling approach for hybrid dimensional metrology to improve the measurement speed and quality. A part is first scanned by the laser scanner to capture the global surface data. And the part is then probed by a tactile sensor where the probing points are dynamically determined to reduce the measurement uncertainty according to the scanned data. The surface model is incrementally updated by using Kalman filter to fuse the contact probed data. Li *et al.* [27] presented a multi-sensor digitization approach by using a tactile probe to compensate the data from a laser line scanner for rapid and accurate RE of geometric features. In this method, the laser line scanner is applied to digitize the global surface of the part, intelligent feature recognition and segmentation algorithms are exploited to extract the geometric elements of the object from the data obtained by the laser scanner. Then, the key feature is re-measured by touch trigger probe with a small number of sampling points. The obtained high precision data can be subsequently used to compensate the point data patches obtained by a laser scanning system. The method has been proven to work for geometric elements, but the solution for free-form surface digitization is not discussed. Ren *et al.* [28] developed a weighted least square based multi-sensor data fusion method for free-form surface measurement. The proposed method is capable of fusing multi-sensor measured datasets with notable reduction of the measurement uncertainty. However, the method still needs a large number of contact measurement points, which makes the measurement efficiency still limited. Colosimo *et al.* [29] achieve multi-sensor data fusion for dimensional and geometric verification with Gaussian process models. The proposed method involves the use of Gaussian processes as modeling tool to correct high-density, low-quality data with low-density, high-quality data. The experimental results show that the proposed method improves the quality of the original

TABLE 1. The system components.

Equipment	Specifications
CNC machine tool	Working volume (mm): 1210× 650 × 600 Positioning accuracy: 5μm Repeating positioning accuracy: 3μm Controller: TSNC-A1M (Independent intellectual property rights)
Touch trigger probe	Renishaw OMP400, Unidirectional repeatability (2σ): ±1 μm
CCD camera	Basler acA2440-20gm Dimension of a pixel:3.45 μm×3.45 μm Resolution: 2448(H) × 2048(V)
Lens	FL-CC1214A-2M Focal length: 12 mm.
Laser	Wavelength: 659.3nm, laser power: 38.1mW, laser current: 116.2mA
PC	Inter(R) Core(TM) i3-3240M, 3.40GHZ, 4 GB RAM

single-sensor datasets. Rak *et al.* [30] developed a method to fusion the high-density low-accuracy data and low-density high-accuracy data by finding and aligning the corresponding points pairs of the two data sets. The experimental results show that the method improves the measurement accuracy to a certain extent, but the measurement accuracy is still limited.

It can be seen that, from the existing multi-sensor integration principle, most of the research work is focused on the cooperation or complementary of multi sensors. The integration of different digitization sensors is limited at the physical level and flexibility level. The intelligent aggregation of the information from different sensors is rarely investigated. The issue of how to give full play to complementary advantages of different sensors and improve the accuracy of fused data through information aggregation is still a challenge, especially for the digitization of free-form surface.

This paper presents an effective approach to perform rapid and accurate reverse engineering of complex objects with the integration of a laser scanner and a tactile probe. The proposed system is unique in that it not only includes the physical integration of the two sensors but also includes their combination at the measurement information level. The aim is to realize the rapid and high precision digitization of complex geometry, by the advantages deriving from the integration of both the optical and the mechanical sensors.

The contribution of this paper can be summarized as follows:

1) A competitive multi-sensor approach for rapid and precise reverse engineering of complex geometry is proposed in this paper. The proposed multi-sensor system is unique in that it includes not only the physical integration of different sensors but also their combination at the measurement information level.
2) A simple and effective point cloud segmentation method is proposed to divide the point cloud into several smooth data patches for surface fitting and data fusion purposes.
3) A multi-sensor data fusion algorithm for geometric surface inspection is proposed, which can improve the optical measurement accuracy to the contact measurement accuracy.
4) A novel shape-preserving curve deformation algorithm is proposed for multi-sensor measurement data fusion of free-form surface. This data fusion method can improve the accuracy of optical measurement with only a small number of contact measuring points, thereby, realize rapid and precise inspection of free-form surface.

The remainder of this paper is organized as follows: The configuration and working principle of the integrated system is introduced in Section II. Section III gives a brief introduction to the coordinate system unification of the multi-sensor measurement system. Section IV provides a simple and effective point cloud segmentation method. The proposed data compensation methods for different types of surface features are presented in Section V. Experimental results are demonstrated in Section VI. Section VII draws the conclusion and perspective of this work.

II. DESCRIPTION OF THE PROPOSED METHOD

The integrated system is designed and manufactured with the following components listed in Table. 1.

Fig. 1 shows a photograph of the prototype measuring device. The five-axis CNC machine tool provides an accurate and repeatable platform from which different digitizers can be gathered. A composite probe is designed, which integrates contact probe and line structured light vision sensor. The contact probe and line structured light vision sensor are fixed on two sides of the substrate through brackets, respectively. Three standard balls are fixed on the worktable of the CNC machine tool for the unification of the coordinate system of the two sensors. When working, the composite probe is mounted on the machine tool spindle and driven by the moving mechanism of the machine tool to digitize the surface of the object. The rotary table of the machine tool helps realize the scanning in any direction.

Fig. 2 shows the measurement model of line structured light vision system. $O_w - X_wY_wZ_w$ is the world coordinate system, $O_c - X_cY_cZ_c$ is the camera coordinate system, $O_u - uv$ is the image coordinate system, O_i is the principal point, and O_c is the optical center. The light plane projected by the

FIGURE 1. Photograph of the prototype measuring device.

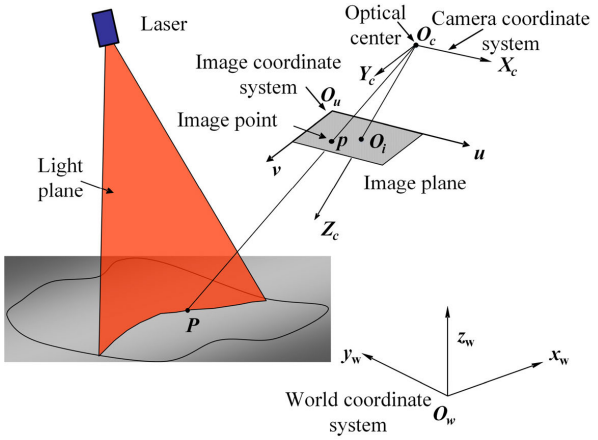

FIGURE 2. Mathematical model of line structured light vision measurement.

laser projector intersects with the surface of the object to be measured to form a characteristic light strip. P is a point on the characteristic light strip, its image on the image plane is p. The spatial position of the point P can be expressed by a ray and a light plane. The coordinates of image point p on the image plane can be obtained by image processing. According to the camera model, the image coordinates of p uniquely correspond to a ray passing through the optical center of the camera, that is, the equation of the ray in the camera coordinate system can be obtained. If the equation of the light plane in the camera coordinate system can be obtained, the coordinates of the point P in the camera coordinate system can be uniquely determined by the ray equation and the light plane equation.

Let the world coordinates of point P be (X_w, Y_w, Z_w), the camera coordinates of point P be (X_c, Y_c, Z_c), and the image coordinates of point p be (u, v). Then the camera model of line structured light vision system can be expressed as

$$\rho \begin{bmatrix} u \\ v \\ 1 \end{bmatrix} = A \left[R_c^w \mathrm{T}_c^w \right] \begin{bmatrix} X_w \\ Y_w \\ Z_w \\ 1 \end{bmatrix} = \begin{bmatrix} f_x & 0 & u_0 \\ 0 & f_y & v_0 \\ 0 & 0 & 1 \end{bmatrix} \begin{bmatrix} r_1 & r_2 & r_3 & t_x \\ r_4 & r_5 & r_6 & t_y \\ r_7 & r_8 & r_9 & t_z \end{bmatrix} \begin{bmatrix} X_w \\ Y_w \\ Z_w \\ 1 \end{bmatrix}, \rho \neq 0 \tag{1}$$

where, A is the camera's intrinsic parameter matrix, f_x and f_y are the effective focal lengths in X and Y directions, respectively. (u_0, v_0) is the coordinates of the principal point. R_c^w and T_c^w represent rotation and translation transformations from the coordinate system $O_w - X_w Y_w Z_w$ to the coordinate system $O_c - X_c Y_c Z_c$, respectively.

The light plane in $O_w - X_w Y_w Z_w$ can be expressed as

$$a_w X_w + b_w Y_w + c_w Z_w + d_w = 0 \tag{2}$$

Equation (1) and (2) represent the mathematical model of the line structured light vision measurement system. In the world coordinate system $O_w - X_w Y_w Z_w$, the ray equation is determined by (1), the light plane equation is determined by (2). Therefore, the three-dimensional world coordinates of point P can be uniquely determined by the intersection of $O_c p$ and light plane.

Fig. 3 illustrates the flowchart of the presented inspection process. With the coordinate data acquired using the laser scanner, a data segmentation and recognition algorithm is proposed to group the data points into two types of data sets: geometric elements and free-form surfaces. These key features of elements are re-measured by tactile probe with a small number of sampling points. Then different data fusion algorithms are proposed to compensate the point data patches which are measured by a laser scanning system. For geometric elements, the least squares method is applied to the contact measurement data points to best fit these geometric elements to derive the parameters. Then each point measured by the laser scanner is compensated according to the derived geometric parameters. For free-form surfaces, slicing operation is firstly conducted on the data patch to extract the section contour curves of the surface patch. Then a shape-preserving curve modification algorithm is proposed to improve the accuracy of the section contour curves obtained by optical measurement. Finally, the compensated data patches are recombined and exploited for accurate reverse engineering of a CAD model. The proposed method uses geometric information obtained from optical measurement to guide contact measurement, and then uses a small amount of high-precision contact measurement data to improve the accuracy of dense optical measurement data. Through the fusion of measurement information from different sensors, the rapidity of optical measurement and high-precision of contact measurement can be brought into full play, thus realizing high-speed and high-precision measurement of complex geometry.

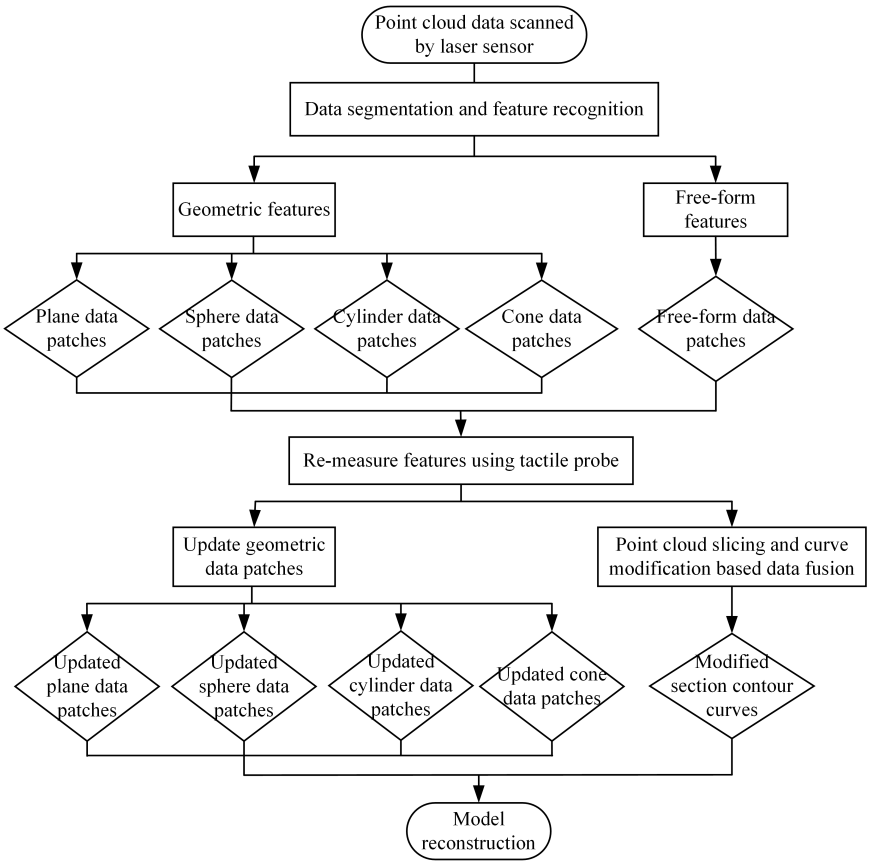

FIGURE 3. Overview of the proposed method.

III. COORDINATE SYSTEM UNIFICATION

Before the unification process, the optical scanner and the contact probe work in their own separate coordinate systems. For multi-sensor data fusion, these two coordinate systems have to be unified. This operation has to be done before any measurement task and carried out only once before a series of measurements. Here, an existing commonly used strategy is adopted for multi-sensor coordinate system unification [31].

As shown in Fig. 1, a calibration board with three standard balls attached to it is fixed on the machine tool worktable. The three standard balls are digitized by the optical scanner and the contact probe separately. The coordinate of each spherical center is calculated, and then the coordinate system alignment of multi-sensor system is realized by aligning the three spherical centers in different coordinate systems [31]. The result of this process is a transformation matrix, which modifies (rotates and translates) the point's coordinates from the optical scanner's relative coordinate system to the absolute system of the contact probe:

$$W_c = R \cdot W_s + T \tag{3}$$

where W_c is the data obtained by the contact probe, W_s is the data obtained by the optical scanner, R is the rotation matrix, and T is the translation vector.

IV. POINT CLOUD DATA SEGMENTATION AND FEATURE RECOGNITION

After a part is scanned, the segmentation process should be conducted on the acquired point cloud data to divide point cloud data into several smooth data patches, each of which logically belongs to a single primitive surface. In this paper, a simple and effective point cloud segmentation and feature recognition method is proposed.

A. EDGE POINTS IDENTIFICATION

Principal component analysis (PCA) of the covariance matrix of a local neighborhood is widely used to estimate local surface properties, such as normal and curvature [32]. Assuming that the point cloud $P = \{p_i\}_{i=1}^{N}$ is sampled from piecewise smooth surfaces, p_i is a point on this surface, and let N_i be the neighborhood of p_i. For each point p_i, a neighborhood N_i of size K_0 is computed. The corresponding covariance matrix C is defined as:

$$C = \begin{bmatrix} p_1 - \bar{p} \\ \cdots \\ p_{K_0} - \bar{p} \end{bmatrix}^T \cdot \begin{bmatrix} p_1 - \bar{p} \\ \cdots \\ p_{K_0} - \bar{p} \end{bmatrix}, \quad p_{i=1,K_0} \in N_i \tag{4}$$

where, $\bar{p}$ is the centroid of the set of neighbors in N_i.

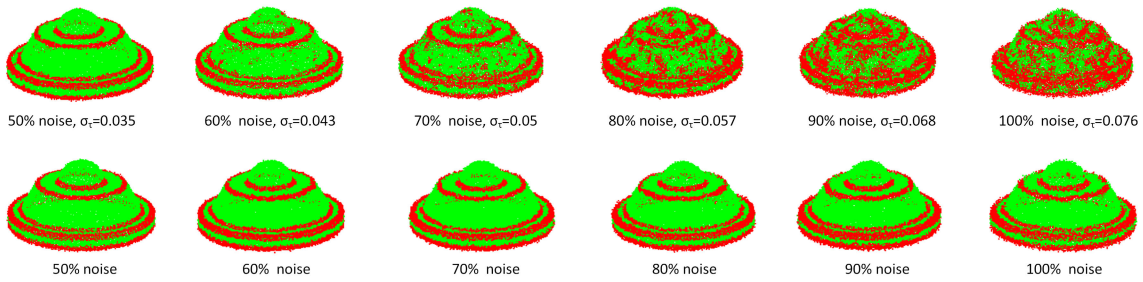

FIGURE 4. The result of edge point identification using PCA and our algorithm at different noise scales. The top row is the result of PCA method and bottom row is the result of our method.

The eigenvalues $\{\lambda_0, \lambda_1, \lambda_2\}$ of the covariance matrix can be estimated by analyzing the following eigenvector problem:

$$C \cdot \bar{v}_j = \lambda_j \cdot \bar{v}_j, \quad j \in \{0, 1, 2\} \tag{5}$$

where $\{v_0, v_1, v_2\}$ are corresponding eigenvectors.

Assume that $\lambda_0 < \lambda_1 < \lambda_2$, then the surface variation σ_i of the underlying surface at the point p_i and an initial normal n_i can be estimated. The surface variation σ_i is defined as:

$$\sigma_i = \frac{\lambda_0}{\lambda_0 + \lambda_1 + \lambda_2} \tag{6}$$

The normal n_i is defined as the eigenvector v_0 corresponding to the smallest eigenvalue λ_0.

In [33]–[35], σ_i is considered as curvature and used to distinguish edge points, who have a more complicated neighborhood, from non-edge points. The coefficient of a point near sharp features is considered to be larger than that of a point in smooth regions. Therefore, each point p_i with σ_i greater than a threshold σ_τ is viewed as an edge point.

However, it has been shown that PCA is sensitive to noise and outliers due to using the classic covariance matrix. As a result, attributes calculated through PCA are highly sensitive to noise and outliers [36]. To improve the accuracy and robustness of edge point recognition, a statistics-based edge point recognition strategy is proposed in this paper. For each point p_i, the initial normal is computed using PCA mentioned above, and then the standard deviation of the point normal values within the point's K_1 neighborhood is computed. The standard deviation of point normal is calculated by:

$$\begin{aligned}\sigma_{ni} &= \left| \sqrt{\frac{\sum_{j=0}^{K_1} n_j - \bar{n}_i}{K_1}} \right| \\ &= \sqrt{\frac{\sum_{j=0}^{K_1} (n_{jx} - \bar{n}_{ix})^2 + \sum_{j=0}^{K_1} (n_{jy} - \bar{n}_{iy})^2 + \sum_{j=0}^{K_1} (n_{jz} - \bar{n}_{iz})^2}{K_1}}\end{aligned} \tag{7}$$

where $\bar{n}_j$ is the unit normal vector of each point in p_i's neighborhood. $\bar{n}_i$ is the average normal vector calculated from the normalized point normals within p_i's neighborhood by:

$$\bar{n}_i = \sum_{j=0}^{K_1} n_j / K_1 \tag{8}$$

The standard deviation of points' normals in a neighborhood indicates the level of changes in the shape of the underlying surface at the point p_i. Each point p_i with normal standard deviation larger than the user-defined threshold $\sigma_{n\tau}$ is viewed as an edge point. In this way, the edge points are identified by statistical analysis of all points' normals in the neighborhood, which is more robust than judging only by the curvature of a single point.

Fig. 4 shows the result of edge point identification using PCA and our algorithm at different noise levels. It can be seen that when the noise level is up to 70%, the PCA-based method fails to accurately identify edge points. Large tracts of points in smooth regions are mistakenly identified to be edge points. On the contrary, our statistics-based method shows good robustness to noise, it can accurately identify feature points under different noise levels.

B. ROUGH SEGMENTATION

Through the edge point identification algorithm mention in Section III.A, each point p_i is identified as edge point or non-edge point according to the standard deviation of the normal vectors of p_i's neighbors (Fig. 5b). For convenience, the set of edge points is donated as P_e and the set of non-edge points is donated as P_n. In the rough segmentation stage, all the edge points are removed from the original point cloud P and the remaining non-edge points P_n are naturally divided into several separated point sets in space domain, as shown in Fig. 5c. Then Euclidean distance clustering [37] is used to segment the non-edge points set into several smooth data patches, each of which logically belongs to a single primitive surface, as shown in Fig. 5d.

C. REFINING SEGMENTATION

Through rough segmentation, the non-edge points set is divided into several meaningful data patches, but the edge points have not yet been assigned to any data patches. To ensuring the integrity of the reconstructed surface, we propose a patch expand procedure to assign each edge point

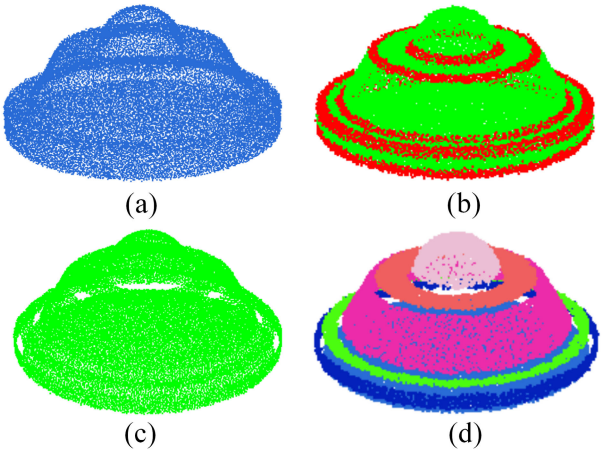

FIGURE 5. Diagram of rough segmentation. (a) Original point cloud data. (b) Result of feature point detection. (c) Point cloud data after removing feature points. (d) Result of rough segmentation.

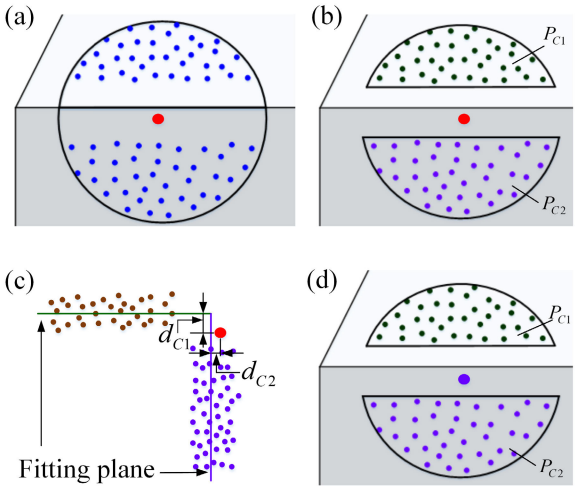

FIGURE 6. The pipeline of patch expansion. (a) Neighborhood of edge point p_i, (b) The neighborhood is divided into several sub-neighborhoods according to which data patches do the non-edge points belong to, (c) Each sub-neighborhood is fitted into a plane and the corresponding deviation from p_i to the fitting plane is computed, (d) p_i is judged belong to P_{C2} according to the deviation to the fitting plane.

to the corresponding point data patch to achieve complete segmentation. For each removed edge point p_i we first add it to the remaining non-edge point set P_n. Then a neighborhood N_i of size K is computed (Fig. 6a) and the neighborhood is divided into several sub-neighborhoods according to which data patches do the non-edge points included in neighborhood N_i belong to, the divided sub-neighborhoods are denoted as $\{P_{C_i}\}$(Fig. 6b). For each point set P_{C_i}, a least squares fitting plane is computed by analyzing its covariance matrix, and the deviation d_{Ci} from current edge point to the fitting plane is also computed (Fig. 6c). Finally, the data patch corresponding to the minimum deviation is considered to be the one to which the current edge point belongs and the current edge point is added to the data patch (Fig. 6d). The results of the data patches before and after expansion are

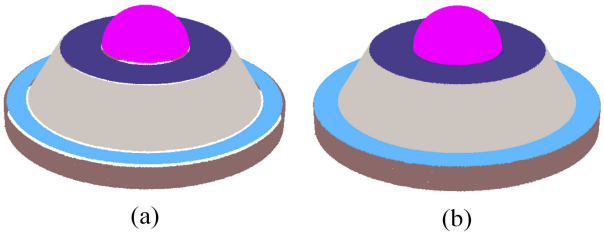

FIGURE 7. Comparison of results before and after patch expansion. (a) Before patch expansion display. (b) After patch expansion display. The patches are marked by different colors.

displayed in Fig. 7. The resulting data patches exhibit significant expansion in space and the point cloud is completely segmented, as shown in Fig. 7b.

The segmentation algorithm presented in this paper can deal with all types of feature surfaces with sharp edges. Our algorithm can not segment the data patches containing surfaces with a smooth transition, because no edge points will be detected. But this does not affect the ultimate effect of our approach, because our feature recognition algorithm will recognize such data patches as free-form surfaces. Therefore, such data patches are treated as free-form surfaces in this paper.

D. FEATURE RECOGNITION

After data segmentation, the point cloud data are divided into several smooth data patches, each of which logically belongs to a single primitive surface. Feature recognition of point cloud patches is necessary for multi-sensor data fusion in this paper. Wang *et al.* [38] propose a random sample consensus (RANSAC) algorithm for point cloud data feature recognition. RANSAC method is a statistical-based approach, which can accurately identify the features of point cloud data patches and derive the expression of features even if the data patches contain a large number of outliers. Therefore, Wang's RANSAC algorithm is adopted for feature recognition in this paper.

V. MULTI-SENSOR DATA FUSION

After data segmentation and feature recognition, the point cloud data are grouped into two types of data sets: geometric features and free-form surfaces. To improve the overall measurement accuracy of integrated system, different data fusion algorithms are proposed to compensate for these two types of data patches.

A. DATA FUSION FOR GEOMETRIC FEATURES

1) PROPOSED METHOD

The geometric features studied in this paper are planes, spheres, cylinders, and cones. Due to their simple mathematical description, a small number of discrete high accuracy point data measured by the tactile probe can be used to fit these geometric elements to precisely derive the parameters. The densely scanned data patches can then be compensated according to the derived parametric expressions.

The specific steps are as follows:

1) Laser scanning is carried out on the entire surface of the part, and then a segmentation and feature recognition algorithm is exploited to group the point cloud into data patches, each of which logically belongs to a single primitive surface.
2) The tactile probe is used to re-measure each geometric feature with a small number of points. Then the obtained high precision points are used to fit these geometric elements to derive the parameters through least squares method.
3) For a data patch that belongs to a plane, substituting the x and y coordinates of each point into the derived parametric equations, and then new z coordinate with higher precision can be obtained. For data patch belonging to cylinder or cone, each point is moved along the radius direction of the fitting surface's cross-section circle so that the distance from the point to the circle center equals its radius. For data patches belonging to spheres, each point is moved along the radius direction of the fitting sphere so that the distance from the point to the sphere center equals the sphere radius.
4) Each point measured by the laser scanner is updated by the algorithm described in step 3, and then a new compensated data set is built. In theory, the compensated data sets have the same accuracy as the data measured from the tactile probe. Therefore, the quality of the point data measured from the optical sensor will be greatly improved.

2) ALGORITHM DESCRIPTION

The detailed algorithms for data fusion of different geometric features are presented as follows:

- DATA FUSION FOR PLANE
  A space plane can be specified by a point (x_o, y_o, z_o) on the plane and the direction cosines (a, b, c) of the normal to the plane. Any point (x_i, y_i, z_i) on the plane satisfies:

$$a\,(x_i - x_o) + b\,(y_i - y_o) + c\,(z_i - z_o) = 0 \tag{9}$$

  Here, we define $d = -(ax_o + by_o + cz_o)$. According to the proposed method, the new z coordinate can be derived by:

$$z_{Ni} = (-ax_i - by_i - d)\,/c \tag{10}$$

- DATA FUSION FOR SPHERE
  A sphere is specified by its center (x_o, y_o, z_o) and radius r. Any point (x_i, y_i, z_i) on the sphere satisfies the equation:

$$(x_i - x_o)^2 + (y_i - y_o)^2 + (z_i - z_o)^2 = r^2 \tag{11}$$

  For sphere compensation, we first translate a copy of the data so that the center of the sphere is at the coordinate origin:

$$(x_i, y_i, z_i) = (x_i, y_i, z_i) - (x_o, y_o, z_o) \tag{12}$$

  Then, the value of the new coordinate of (x_i, y_i, z_i) can be derived by:

$$(x_{Ni}, y_{Ni}, z_{Ni}) = (x_i, y_i, z_i) + (r - \sqrt{x_i^2 + y_i^2 + z_i^2}) * \frac{(x_i, y_i, z_i)}{\sqrt{x_i^2 + y_i^2 + z_i^2}} \tag{13}$$

  Finally, the updated data is translated back by an amount equal and opposite to the vector in (9), above.
- DATA FUSION FOR CYLINDER
  A cylinder can be specified by a point (x_o, y_o, z_o) on its axis; a vector (a, b, c) pointing along the axis and its radius r.
  For cylinder and cone compensation, we first conduct translation and transform on the data so that the point (x_o, y_o, z_o) on the axis lies at the coordinate origin and the vector (a, b, c) coincides with z-axis. Again, we will translate and rotate the data back after compensation. Then for any point (x_i, y_i, z_i), the value of the new x, y coordinate can be obtained by:

$$(x_{Ni}, y_{Ni}) = (x_i, y_i) + (r - \sqrt{x_i^2 + y_i^2}) * \frac{(x_i, y_i)}{\sqrt{x_i^2 + y_i^2}} \tag{14}$$

  Finally, the updated coordinate data is (x_{Ni}, y_{Ni}, z_i).
- DATA FUSION FOR CONE
  A cone can be specified by a point (x_o, y_o, z_o) on its axis; a vector (a, b, c) pointing along the axis; the apex semi-angle ϕ and the radius r at the point (x_o, y_o, z_o).
  After data set translation and rotation, the value of the new x, y coordinate can be calculated by:

$$(x_{Ni}, y_{Ni}) = (x_i, y_i) + ((\mathrm{r} - k * (z_i - z_0)) - \sqrt{x_i^2 + y_i^2}) * \frac{(x_i, y_i)}{\sqrt{x_i^2 + y_i^2}} \tag{15}$$

  where $k = \tan(\phi)$. Finally, the updated coordinate data is (x_{Ni}, y_{Ni}, z_i).

B. DATA FUSION FOR FREE-FORM SURFACE

Curve modification has been commonly used for computer aided design of free-form curves and surfaces, in which the process of modification goes on until the shape of the curves and surfaces satisfies the requirements. In this paper, a novel curve modification algorithm based on energy method is proposed for free-form surface measurement data fusion.

The initial curves obtained by optical measurement can reflect the shape of the object surface well. However, there is a slight difference between the measured curves and the actual surface curves due to the low accuracy of optical measurement system. The data points measured by tactile probe are highly precise and these points can be used as constraints to modify the initial section curves obtained by optical measurement to satisfy new position requirements. Through curve modification, the initial section contour curves are revised to

pass through all the high precision tactile probing data and preserve the tendency of the original shape, the accuracy of optical measurement can thus be improved.

In energy-based curve deformation algorithms, the deformation of a curve is realized under the combined action of the internal and external energy of the curve. The internal energy maintains the original shape of the curve, while the external energy provides power for the deformation of the curve.

1) INTERNAL ENERGY OF CURVE

Let $P(u)$ be a space curve parameterized by u, the traditional internal energy of the curve is [39]

$$E_{internal} = \int_{\Omega} \frac{\alpha}{2} \left\| \frac{dP(u)}{du} \right\|^2 + \frac{\beta}{2} \left\| \frac{d^2P(u)}{du^2} \right\|^2 du \quad (16)$$

where α and β are weighting parameters that control the deformable contour's tension and rigidity, respectively. Ω is the parametric domain of the curve.

When the internal energy of the curve expressed by (13) reaches the minimum value, the curve evolves into a straight line, that is, under the action of internal energy, the curve will gradually smooth into a straight line. This form of curve internal energy obviously can not meet the requirements of this paper. The focus of this paper is to achieve curve modification on the basis of maintaining the original shape of the curve as far as possible, that is, the curve internal energy should be shape-preserving.

To this end, a new internal energy of the curve is presented in this paper. Since (13) smoothes the curve into a straight line, when it reaches the straight line state, the internal energy of the curve will be reduced to the extreme value of zero. Based on this, we construct an error curve which satisfies the following equation

$$R(u) = P(u) - S(u) \quad (17)$$

where $R(u)$ is the error curve, $P(u)$ is the deformed curve, $S(u)$ is the original curve before deformation.

In this way, when the error curve satisfies the minimum value of (13), the internal energy of the error curve is zero, that is, the shape of the deformed curve is consistent with that of the original curve, that is to say, the shape of the original curve is preserved.

From (13) and (14), the internal energy for deformed curves is

$$E_{internal} = \int_{\Omega} \frac{\alpha}{2} \left\| \frac{dP(u)}{du} - \frac{dS(u)}{du} \right\|^2 + \frac{\beta}{2} \left\| \frac{d^2P(u)}{du^2} - \frac{d^2S(u)}{du^2} \right\|^2 du \quad (18)$$

Equation (15) makes the deformed curve keep its original shape as much as possible. However, the optical measurement data inevitably contain noise and outliers. In order to make the curve modification algorithm have the ability to smooth noise, this paper further optimizes the curve internal energy into the following forms:

$$E_{internal} = \int_{\Omega} \frac{\alpha}{2} \left\| \frac{dP(u)}{du} - \frac{dS(u)}{du} \right\|^2 + \frac{\beta}{2} \left\| \frac{d^2P(u)}{du^2} \right\|^2 du \quad (19)$$

The meaning of the second integral term of the new internal energy of the curve is to minimize the curvature of the deformed curve. By minimizing the internal energy of the curve, on the one hand, the deformed curve keeps the shape of the original curve under the constraint of the first term of (16), on the other hand, the curvature of the deformed curve is minimized under the constraint of the second term of (16). Therefore, the curve can be smoothed on the basis of maintaining the original shape of the curve, so as to further improve the accuracy of the fused data.

2) EXTERNAL ENERGY OF CURVE

Constructing a new curve that meets the requirements on the basis of the original curve requires imposing various constraints on the curve. These constraints are transformed into external energy of curves. In the field of computer aided design, the most commonly used geometric constraints are displacement constraint and tangent vector constraint. However, for the measurement application scenario in this paper, it is difficult to get the actual tangent vector of the measured surface, so the tangent vector constraint is not applicable to the multi-sensor measurement data fusion, and only displacement constraint is considered.

We construct the external energy with spring-like system. Assuming that there are m high-precision contact measuring points as displacement constraint points, they are expressed as C_i $(i = 1, 2, \cdots m)$, if $P(u_i) = C_i$ is deemed to be the zero-extension location of spring, then the external energy can be written as

$$E_{external} = \sum_i \frac{\gamma}{2} [P(u_i) - C_i] \quad (20)$$

where γ represent the external force stiffness coefficient in a broad sense. Minimizing the external energy will result in $P(u_i) = C_i$, that is to say, the external energy will always tend toward making the resultant curve $P(u)$ satisfy the given conditions.

3) TOTAL ENERGY OF CURVE

The curve modifications are deemed to be the deformations under total energy including both internal energy and external energy. The total energy of curve equals to

$$\begin{aligned} E_{total} &= E_{internal} + E_{external} \\ &= \int_{\Omega} \frac{\alpha}{2} \left\| \frac{dP(u)}{du} - \frac{dS(u)}{du} \right\|^2 + \frac{\beta}{2} \left\| \frac{d^2P(u)}{du^2} \right\|^2 du \\ &\quad + \sum_i \frac{\gamma}{2} [P(u_i) - C_i] \end{aligned} \quad (21)$$

In this paper, uniform cubic B-spline is used to represent the section contour. let $P_k(u) = \sum_{l=0}^{3} B_{3,l}(u) W_{k+l}$ and

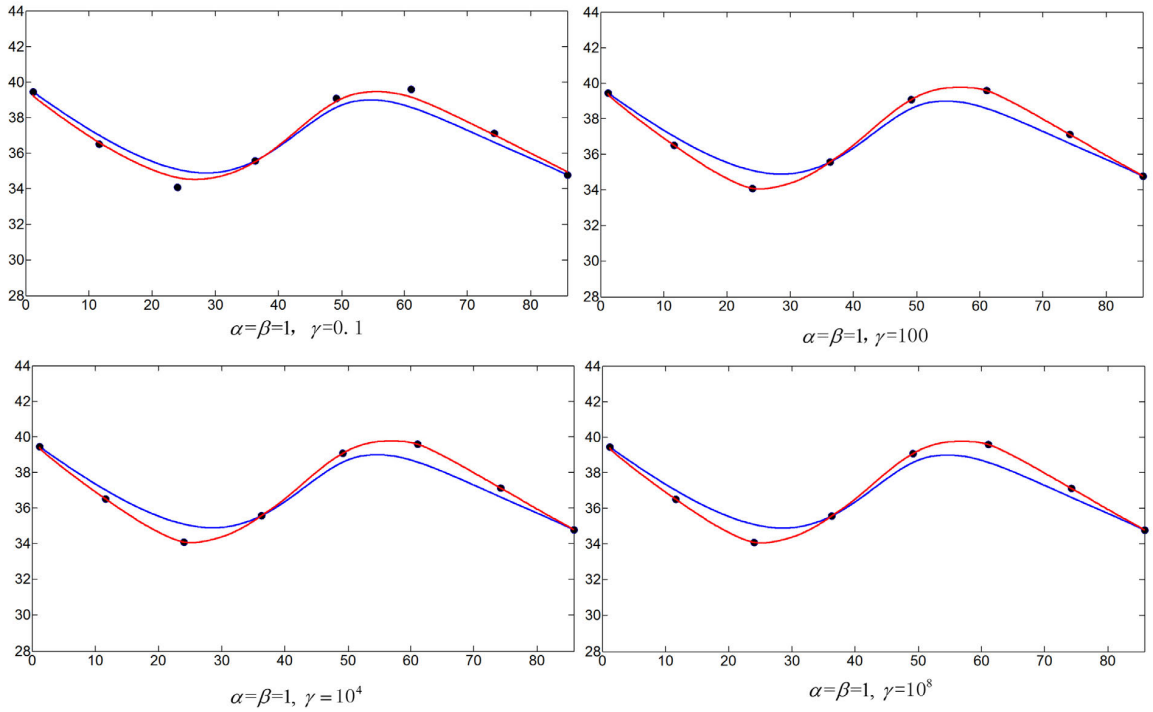

FIGURE 8. The influence of the parameter γ on the results of curve deformation.

$S_k(u) = \sum_{l=0}^{3} B_{3,l}(u) U_{k+l}$, where W_k and U_k denote the control point vectors of the resultant curve and original curve respectively. Equation (18) can be represented as:

$$E_{total} = \sum_{k=1}^{n-1} \int_0^1 \frac{\alpha}{2} \left[\sum_{l=0}^{3} B'_{3,l}(u) W_{k+l} - \sum_{l=0}^{3} B'_{3,l}(u) U_{k+l} \right]^2 du + \sum_{k=1}^{n-1} \int_0^1 \frac{\beta}{2} \left[\sum_{l=0}^{3} B''_{3,l}(u) W_{k+l} \right]^2 du + \sum_i \frac{\gamma}{2} \left[\sum_{l=0}^{3} B_{3,l}(u_i) W_{i+l} - C_i \right]^2 \quad (22)$$

where $B'_{3,l}(u)$ and $B''_{3,l}(u)$ means the first and second derivation of $B_{3,l}(u)$ with respect to the parameter u.

Let $B(u) = \left[B_{3,0}(u), B_{3,1}(u), B_{3,3}(u), B_{3,3}(u)\right]^T$, $X_k = [W_k, W_{k+1}, W_{k+2}, W_{k+3}]^T$, $Y_k = [U_k, U_{k+1}, U_{k+2}, U_{k+3}]^T$, then (19) becomes:

$$E_{total} = \sum_{k=1}^{n-1} \int_0^1 \frac{\alpha}{2} \left[X_k^T B'(u) - Y_k^T B'(u) \right]^2 + \frac{\beta}{2} \left[X_k^T B''(u) \right]^2 du + \sum_i \frac{\gamma}{2} \left[X_i^T B(u_i) - C_i \right]^2 \quad (23)$$

According to the principle of variational calculus, the resultant curve's control points should satisfy the following differential equation:

$$\frac{\partial E_{total}}{\partial W_k} = 0 \quad (k = 1, 2, \ldots, n+2) \quad (24)$$

Through (21), the new control points of the resultant curve can be solved, so the new curve is determined.

4) PARAMETER SELECTION

The parameter selection of α, β, γ has a significant effect on the resultant curve. Usually, these parameters are chosen in different orders of magnitude. For the sake of convenience of comparison, we set $\alpha = 1$. Fig. 8 shows the effect of parameters γ on the curve deformation. The blue curve is the original curve, the red curve is the resultant curve after deformation and the black solid circles are the displacement constraint points. Generally speaking, the optimization problem of (21) can not strictly meet with the given conditions. The larger the value of parameter γ, the better the given condition is satisfied. Therefore, large value of γ is needed to well satisfy the given conditions. However, large value of γ might leads to an unstable solution of (21). A proper value of γ lies roundabout $10^2 - 10^8$.

Fig. 9 shows the effect of the parameter β on the curve deformation. The black curve is a smooth curve without noise, the blue curve is a curve obtained by adding random noise to black curve. The black solid circles are the displacement constraint points. In order to facilitate observation, we select constraint points from the original black curve and shift the Y coordinate of these points downwards by 1 mm, so that the deformed curve will keep the shape trend of the

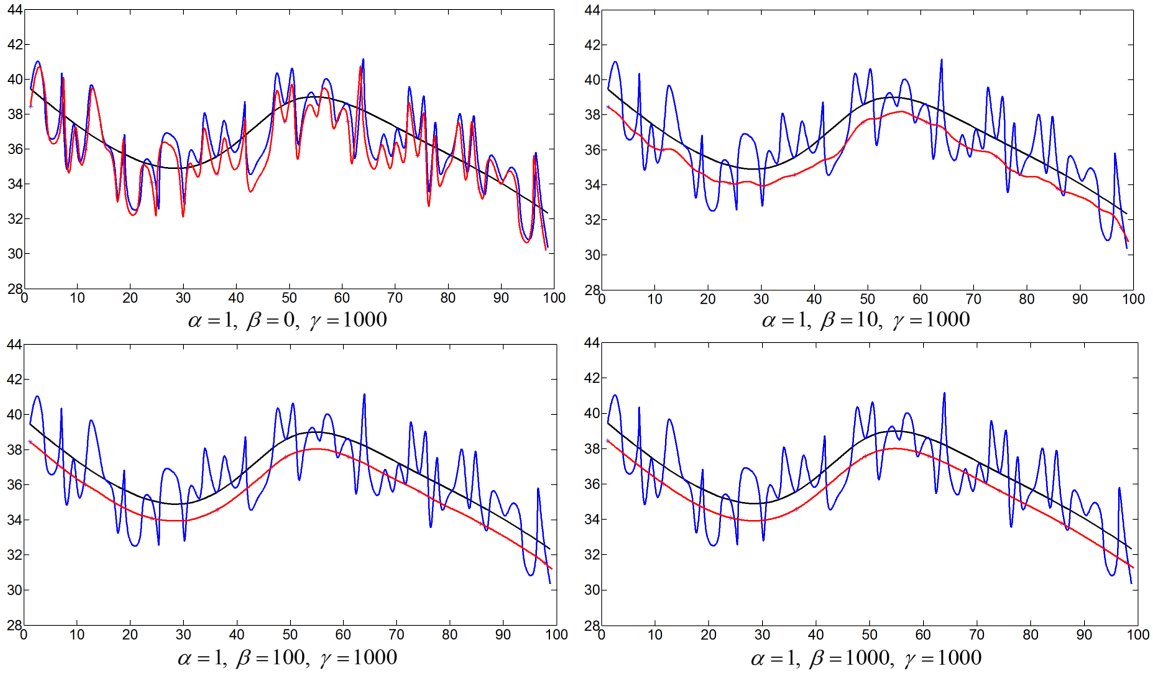

FIGURE 9. The influence of the parameter β on the results of curve deformation.

original curve, which is convenient for comparing the results of the algorithm. The red curve is the resulting curve obtained by applying the curve deformation algorithm proposed in this paper on the blue noisy curve. It can be seen that the greater the value of the parameter β, the smoother the resulting curve is. But too large β value will lead the resulting curve to be excessively smoothed, thus deviating from the overall shape tendency of the original curve. In practice, the value of β should be selected according to the noise level, the bigger the noise scale, the bigger the β value should be, usually, the scope of β is $10^{-1} - 10^{3}$.

VI. EXPERIMENTAL IMPLEMENTATION

In this section, three parts with various geometric features are used to verify the effectiveness of the proposed algorithm. The proposed multi-sensor digitization method was compared to contact measurement and laser scanning methods to validate the advantage and the feasibility.

A. EXAMPLE ONE

Part A (see Fig. 10a) is made of aluminum alloy and designed with only geometric features. The geometric elements on the part include typical geometric features: plane, sphere, cylinder, and cone. The data measured by laser and tactile probe are shown in Fig. 10b, c, respectively. The data measured by the laser scanner is segmented into point data patches each belonging to a different surface patch (see Fig. 10d). Then the large amounts of scattered points that belong to different geometric element patches can be compensated by a small amount of high-precision tactile probing points.

The fitting results for different features using different digitization methods are listed in Table. 2. It can be seen that the quality of the point data measured from laser scanner has been greatly improved after compensation. The compensated data are almost the same as the accuracy of the data measured from the tactile probe. In recent years, with the development and wide application of optical measurement technology, surface reconstruction via large discrete sampling data set has been developed as one of the main research subjects with the wide attention of both theoretical and applied circles. The data fusion method in this paper provides good input data for these algorithms, which improves the accuracy of reconstructed surface. The meshed surfaces from the laser scanning data before and after compensation are illustrated in Fig. 11a, b, respectively. We can see that the surface reconstructed with the compensated data is more smooth and precise.

B. EXAMPLE TWO

To demonstrate the feasibility of the proposed method for free-form surface measurement, a free-form surface of a part made of aluminum alloy with the base measuring 100mm×100mm is served as a test object. The experiment is carried out as follows:

1) VALIDATION POINTS

In order to assess the resulting surface quality of the proposed inspection system, a set of validation points are collected by CMM. The measurements are carried out on a CMM, MPEE = 2.2 + L/350 μm, equipped with a Renishaw PH10M PLUS probe, a 50 mm stylus with a ball tip

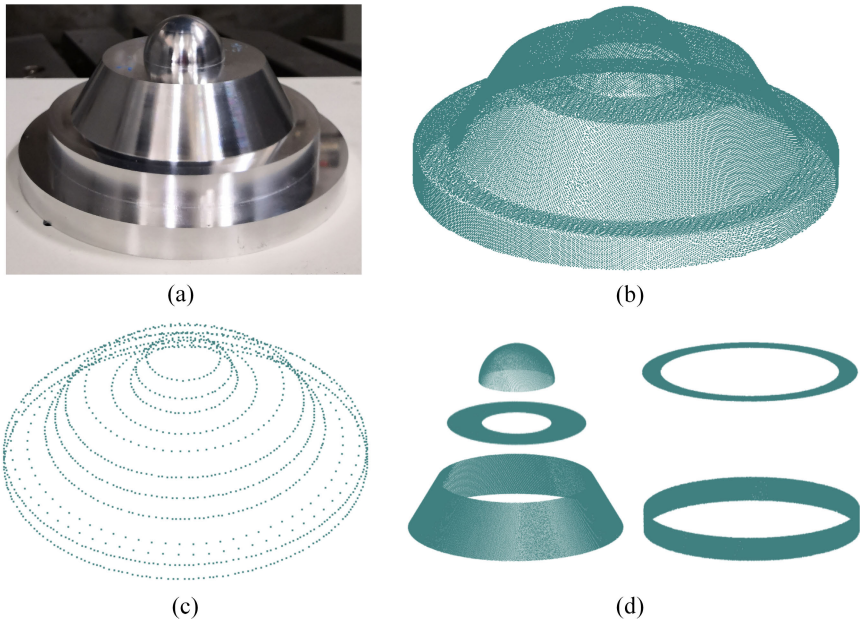

FIGURE 10. Points data measured using multi-sensor system. (a) Part A to be measured. (b) Data measured from laser scanner. (c) Points measured from tactile probe. (d) Segmented data patches.

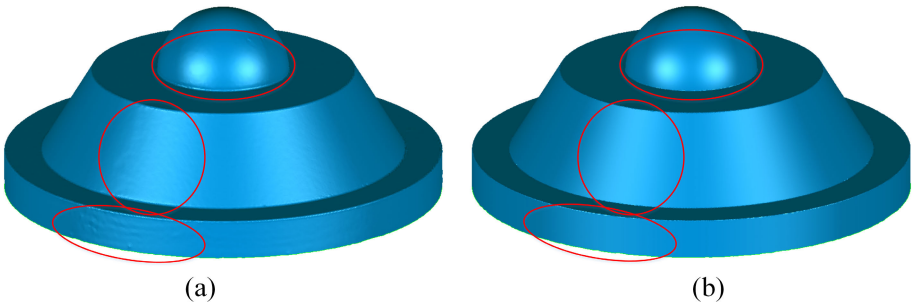

FIGURE 11. Meshed surface. (a) Surface before compensation. (b) Surface after compensation.

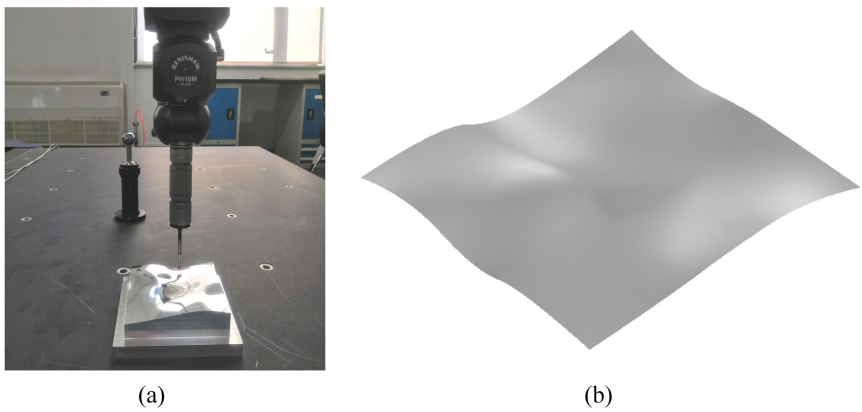

FIGURE 12. Deterministic surface construction. (a) Coordinate measurement using CMM. (b) The fitting surface in CMM inspection.

of 5 mm in diameter. 900 uniformly distributed sampling points are measured along a regular grid u × v (30 rows × 30 columns) in area (0.01–0.99) u × (0.01–0.99) v. Fig. 12a presents the measurement performed on CMM. The inspection data are used to fit the deterministic surface, shown in Fig. 12b.

TABLE 2. Fitting results using different methods (dimensions in mm).

Feature	Parameter	Laser	CMM	Tactile probe on CNC	Compensated
Plane1	points	54092	60	60	54092
	a	0.0000	0.0000	0.0000	0.0000
	b	0.0000	0.0000	0.0000	0.0000
	c	1.0000	1.0000	1.0000	1.0000
	d	9.970	9.9974	9.9974	9.9976
Plane2	points	45664	60	60	45664
	a	0.0000	0.0000	0.0000	0.0000
	b	0.0000	0.0000	0.0000	0.0000
	c	1.0000	1.0000	1.0000	1.0000
	d	29.978	30.000	30.000	30.000
Sphere	Points	34484	60	60	34484
	x0	0.0010	0.0010	-0.0030	-0.0030
	y0	-0.0050	-0.0020	1.5940e-04	1.5940e-04
	z0	29.9908	30.0024	30.0067	30.0067
	r	15.0323	15.0261	15.024	15.0240
Cylinder	Points	52100	60	60	52100
	a	0.0020	0.0000	0.0000	0.0000
	b	-0.0020	0.0000	0.0000	0.0000
	c	1.0000	1.0000	1.0000	1.0000
	r	49.982	49.9736	49.9729	49.9729
Cone	Points	134573	60	60	134573
	a	0.0000	0.0000	0.0000	0.0000
	b	0.0000	0.0000	0.0000	0.0000
	c	1.0000	1.0000	1.0000	1.0000
	Φ	59.4402	59.4845	59.4784	59.4787
	r	47.1663	47.1711	47.1736	47.1736

2) LASER SCANNING

The non-contact digitization of the whole surface is carried out with a laser line scanner, as shown in Fig. 13. As the scanned product is made of aluminum alloy, its surface has the specular properties, which will increase the measurement uncertainty. So, the object is lightly painted with white matte paint before scanning is carried out. The acquired 3D points cloud data are pre-processed for smoothing, reduction, etc., and then serves as a guide for tactile probe.

3) DIGITIZATION USING TACTILE PROBE

After laser scanning, slicing operation is conducted on the point cloud model to extract section contour curves of the measured surface. The principle of point cloud slicing is shown in Fig. 14a. A set of parallel planes are used to slice the point cloud model along a user-defined direction. Supposing the point cloud model is P, one of the section planes is E, the width of its correlated domain is d, where d, or bandwidth, is fixed and is determined by the density of the points. Thus a narrow band, which uses the section plane E as its mid-section, is formed. The points between plane E_l and E make up the point set of down-domain K_l and the points between plane E_r and E make up the point set of up-domain K_r.

Correlated points matching operation is performed between K_l and K_r to find correlated point-pair set with the minimum distance. Section contour point set is then determined by finding intersections between the connecting lines of correlated point-pairs and the section plane, as shown in Fig. 14b.

As shown in Fig. 15, the point cloud model acquired using laser scanning is intersected by 20 parallel section planes with a constant interval. The slicing direction is along the X-axis and several original contour curves are obtained after slicing and B-spline curve fitting. Then, measuring points of contact measurement are determined through equal chord deviation samples on these section contour curves. According to the position and normal vector of each measuring point, it is easy to plan the path of tactile probe and generate G code

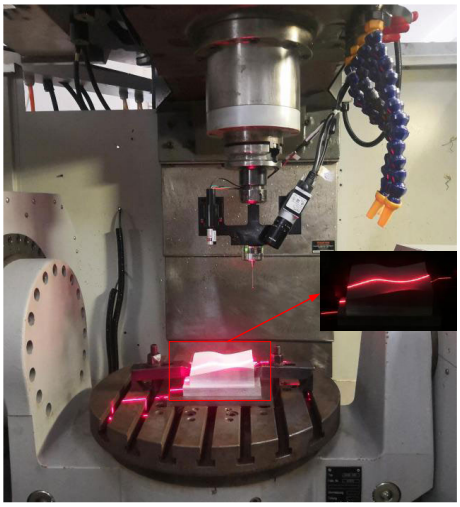

FIGURE 13. Laser scanning on the CNC machine tool.

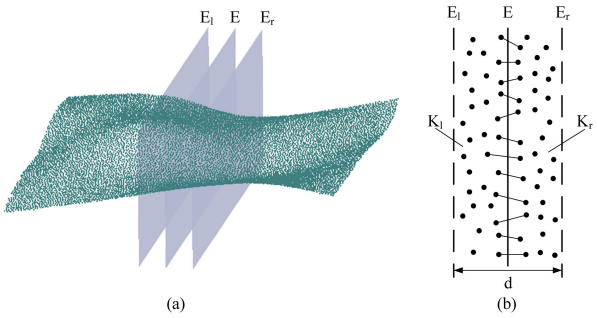

FIGURE 14. Point cloud slicing. (a) Point cloud slicing diagram. (b) Calculation of intersection points.

files that can be executed by CNC machine tool. As shown in Fig. 16, the CNC system controls the moving mechanism of the machine tool to drive the probe move to each measuring position and obtain the coordinate data of the measuring point. These obtained data points are then used to compensate for the data of non-contact digitization.

4) DATA FUSION AND PRECISION ANALYSIS

To improve optical measurement accuracy, the original contour curves are compensated by using the shape-preserving curve deformation technique mentioned in Section IV.B. A total of 227 high precision contact measurement data points are used as constraint points to conduct modification on the initial section contour curves of optical measurement. A series of modified contour curves are then obtained after data fusion, as shown in Fig. 17.

To clearly show the results of the data fusion, the second section curve is particularly analyzed. A total of 100 points are sampled and analyzed from the original section curve, the deformed curve after data fusion, respectively. As shown in Fig. 18a, there are 11 contact measurement data points used as constraint points for curve modification. It can be seen that the original section curve obtained by non-

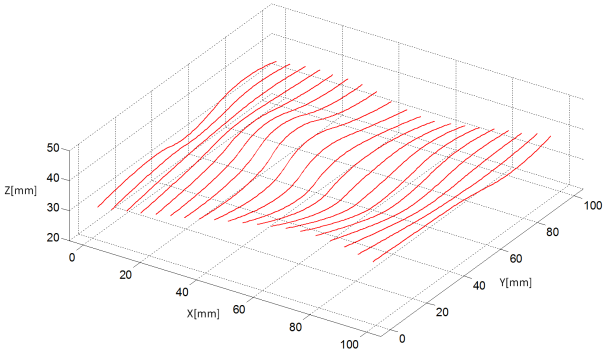

FIGURE 15. The original section curve obtained through point cloud slicing.

FIGURE 16. Contact measurement on the CNC machine tool.

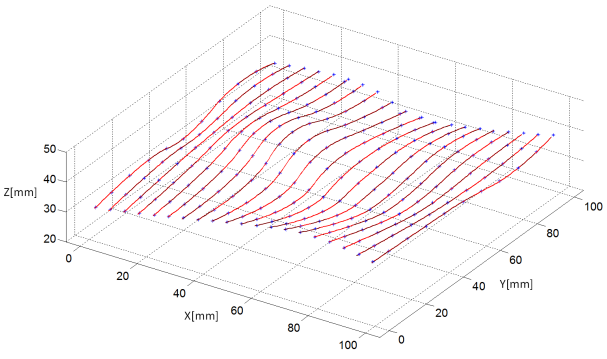

FIGURE 17. Data fusion through curve modification. The original section curves are shown in red, the resultant curves after data fusion are shown in blue, the data points obtained by contact measurement are marked by asterisks.

contact measurement is pulled to the theoretical curve, and the resultant curve passes through all contact measurement data points while maintaining the shape of original section curve. Fig. 18b shows the deviation that corresponds to the

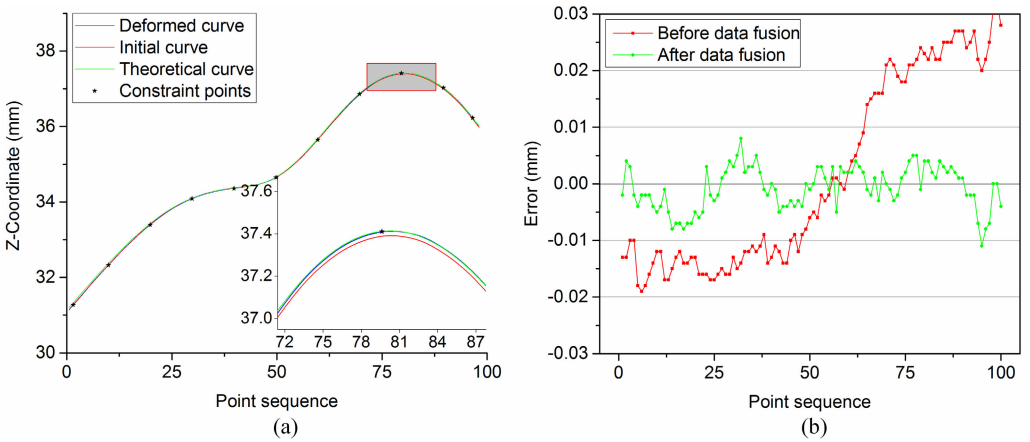

FIGURE 18. Data fusion of the second section curve. (a) Data fusion result of the second section curve. (b) Deviation of the second section curve before and after compensation.

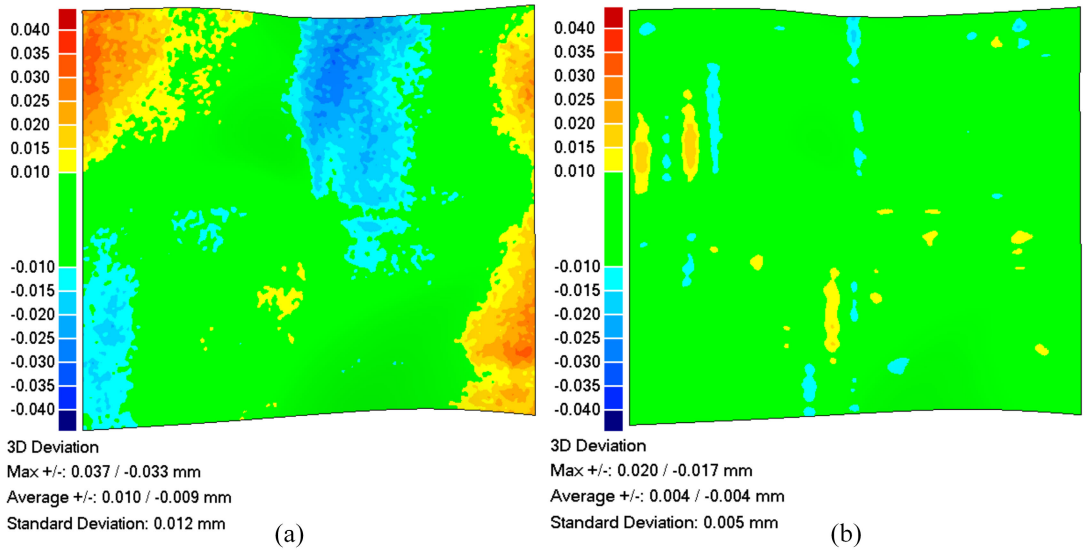

FIGURE 19. Comparison between the reconstructed surface and deterministic surface. (a) Surface reconstructed from raw scanned data. (b) Surface reconstructed from compensated data.

second section curve before and after compensation. The deviation is determined by calculating the difference between the points sampled from the curves and the deterministic surface. It can be seen that the measurement error is greatly reduced after compensation. The maximum error is reduced from +0.032/-0.019 mm to +0.008/-0.011 mm, and the deviations are mainly within ±0.01mm after compensation.

The skinning operation is then carried out on the new section contour curve group to reconstruct the surface after data fusion. To verify the effectiveness of the multi-sensor data fusion algorithm, the original surface from optical measurement and the reconstructed surface after data fusion are compared to the deterministic surface measured using CMM. The comparisons are carried out in Geomagic Qualify (GQ) software, the results of the analysis are shown in Fig. 19. It can be seen that there is a large deviation between the original surface of optical measurement and the deterministic surface, especially in highly curved and edge areas. After the fusion of contact and optical measurement data, the deviation in most areas of the reconstructed surface had been significantly reduced. This shows that the proposed data fusion method can effectively improve the accuracy of optical measurement.

However, it can be seen from Fig. 19b that the errors present zonal distribution between the section planes after surface reconstruction. Especially in the large curvature region, the error is even larger than that before data fusion. The reason for this is that the interval between adjacent section planes is too large to reconstruct the surface with ideal precision using the skinning operation. To further improve measurement accuracy, it is necessary to increase the number of section planes. However, this will also increase the number

TABLE 3. Statistics of experiment results.

Digitization method	Number of points (pts)	Data collection time (s)	Data process time (s)	Total Time (s)	Maximum deviation (mm)	Average deviation (mm)	Standard deviation (mm)
Laser scanning	96640	1:07	0:46	1:53	+0.037/-0.033	+0.010/-0.009	0.012
Contact measurement	900	26:48	0:13	27:01	+0.013/-0.011	+0.003/-0.002	0.003
Multi-sensor digitization	128(CM)+ 96640 (LS)	5:05	1:21	6:26	+0.016/-0.016	+0.004/-0.004	0.004

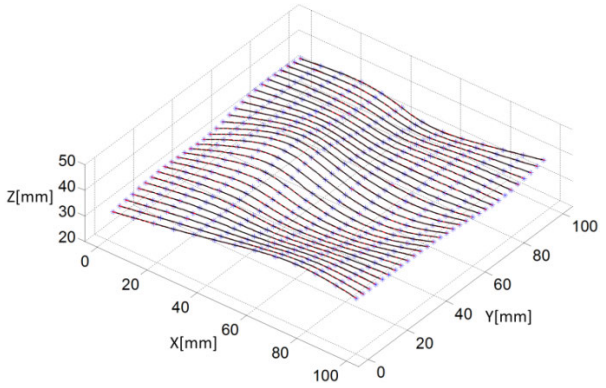

FIGURE 20. The secondary point cloud slicing and data fusion along the Y direction. The original section curves are shown in red, the resultant curves after data fusion are shown in blue, the asterisks represent points on the resultant curves after the first data fusion along X direction.

of contact measuring points and reduce the efficiency of the system.

To cope with this problem, a double-direction data fusion method is proposed in this paper. This method can further improve the measurement accuracy without increasing the number of required contact measurement points. Through the above analysis of the data fusion for the second section curve, it can be seen that the resultant curves after compensation are very precise (Fig. 18b). Therefore, the points on these curves can be used as constraint points for the section contour curves along the Y direction for secondary data fusion. It is noted that 13 constraint points are enough to obtain high precision contour curves through curve modification. Therefore, 13 slicing planes are used to intersect the point cloud model along the X direction firstly, and 13 high precision section contour curves are obtained through data fusion with a total of 128 contact measuring points as constraint points. Then a second application of point cloud slicing along the Y direction with more intensive section planes is performed. With the points on the deformed contour curves along X direction as constraint points, 30 high precision contour curves along Y direction are then obtained, as shown in Fig. 20. Then these newly-constructed section contour curves are used for surface reconstruction.

To verify the validity of the proposed double-direction data fusion method, the reconstructed surface is imported into GQ for error analysis. As shown in Fig. 21a, the deviation between the reconstructed surface and the deterministic surface was further reduced after secondary data fusion. The deviation was reduced to ± 0.016 mm in most areas. To further demonstrate the advancement of our approach, we compared the measurement result with a commercial measuring device. The commercial measuring device used here is HandySCAN 700 from Creaform Company with accuracy of 0.03 mm and volume accuracy of 0.020mm + 0.025mm/m. Fig. 21b shows the comparison between surface reconstructed from measurement data of commercial device and deterministic surface. It can be seen that the measurement accuracy of the proposed method is obviously higher than that of commercial non-contact measuring equipment. The proposed method compares favorably with commercial equipment in terms of various error statistics, which further proves the superiority and effectiveness of the proposed algorithm.

Fig. 22 shows the dispersion curves and the standard deviation obtained for the comparative analysis in GQ between the deterministic surface and the original surface of optical measurement and the surface reconstructed from double-direction data fusion. It can be observed that the deviation of optical scanning data is mainly distributed from -0.015 mm to +0.015 mm, and the deviation interval is reduced to -0.008 mm - $+0.008$ mm after secondary data fusion. In addition, standard deviation (and therefore the uncertainty) is also reduced to a very low level after data fusion.

5) THE FINAL STATISTICS OF THE EXPERIMENT RESULTS

The final statistics of the experiment results are listed in Table. 3. Our novel multi-sensor method spent much less time on the data collection than contact measurement because only a small number of contact measuring points are needed. However, much more time is spent on data processing. That is because the data pre-process and fusion of the two sensors are relatively complex. In terms of reconstruction accuracy, multi-sensor digitization can achieve much more accurate measurements than laser scanning, but the accuracy is slightly lower than that of contact measurement. The reason for this is that the systematic error of optical measurement can be corrected through data fusion. Therefore, the accuracy of multi-sensor measurement is better than pure optical measurement. However, the proposed data fusion method is based on global curve modification, and local distortions of contour curves that are caused by random errors of optical measurement cannot be completely corrected, which makes the accuracy of multi-sensor measurement slightly lower than that of contact measurement.

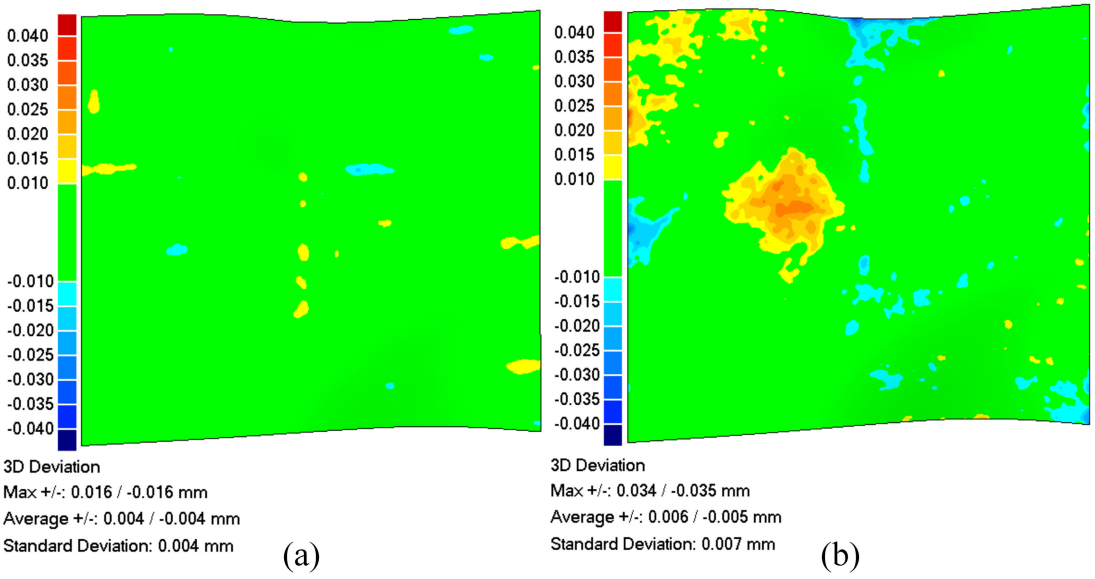

FIGURE 21. Comparison between the reconstructed surface and deterministic surface. (a) Surface reconstructed from double-direction data fusion. (b) Surface reconstructed from measurement data of commercial measuring equipment.

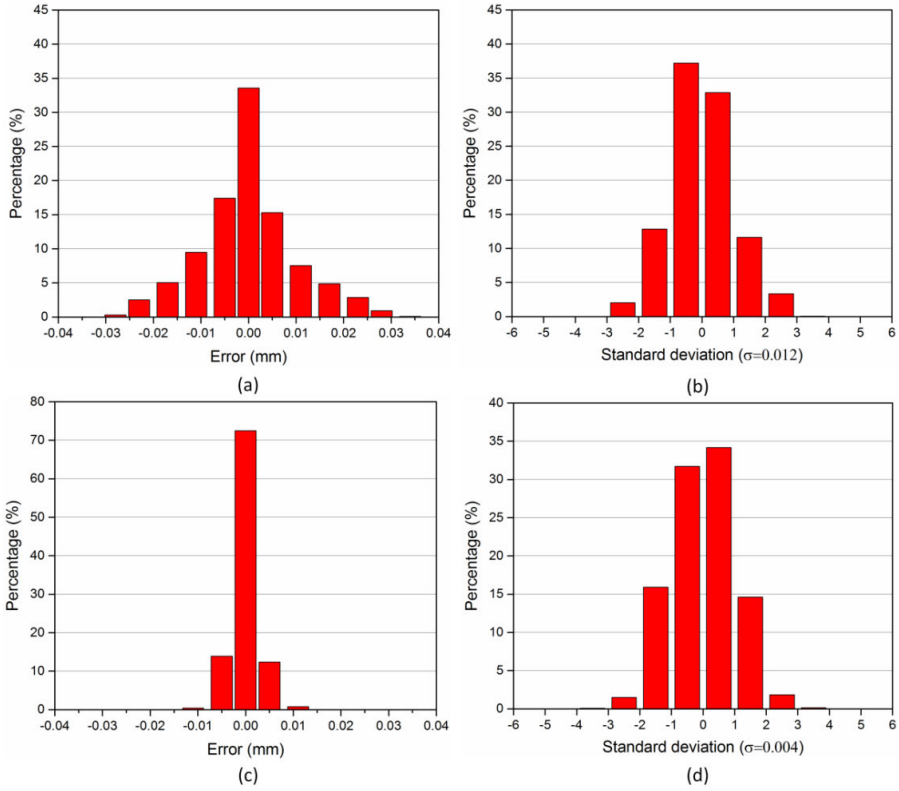

FIGURE 22. Curves of distributions and standard deviations of the reconstructed surface with original scanning data (top row) and surface reconstructed from data compensated by double-direction data fusion (bottom row). (a) and (c) Percentage of error distribution. (b) and (d) Standard deviation.

Consequently, taking the actual total time and accuracy of the resulting surface into consideration, our multi-sensor digitization method achieved an optimal performance both in accuracy and working time among the three digitization methods. Therefore, the experiment results indicate that rapid and precise reverse engineering can be

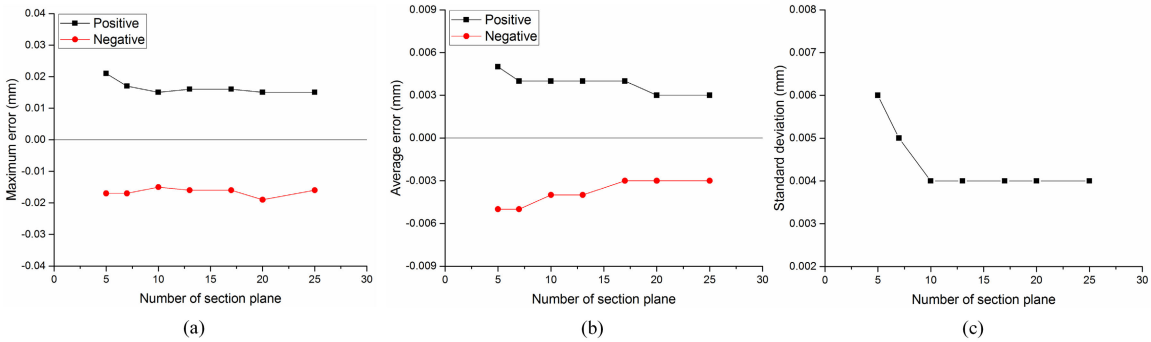

FIGURE 23. Influence of the number of section planes on accuracy. (a) Maximum error. (b) Average error. (c) Standard deviation.

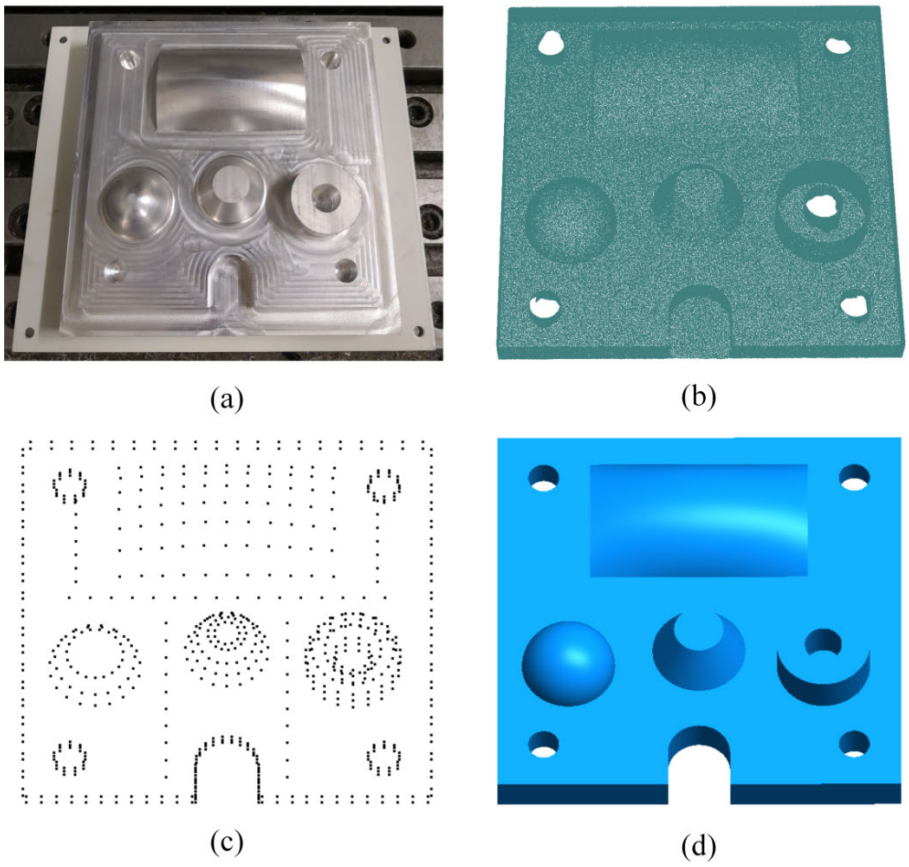

FIGURE 24. RE of part C. (a) Part C to be measured. (b) Points data scanned from the laser scanner. (c) Data captured by the tactile probe. (d) CAD model constructed in solidworks.

achieved by the proposed approach for complex free-form surface.

6) INFLUENCE OF THE NUMBER OF SECTION PLANES ON ACCURACY

To see the effect of the number of section planes on surface reconstruction accuracy, we slice the point clouds with different number of section planes, the reconstructed surfaces are compared with the deterministic surface. Fig. 23 shows that with the increase of the number of section planes, the accuracy of reconstructed surface is improved, but when the number of section planes increases to a certain value, the accuracy of reconstructed surface remains almost constant. Intuitively, more section planes are needed for a freeform surface with larger surface slope.

7) DETERMINATION OF SECTION PLANE

To determine the number and location of the section plane, we can first slice the point cloud along the Y direction to obtain dense section curves. And then we determine the

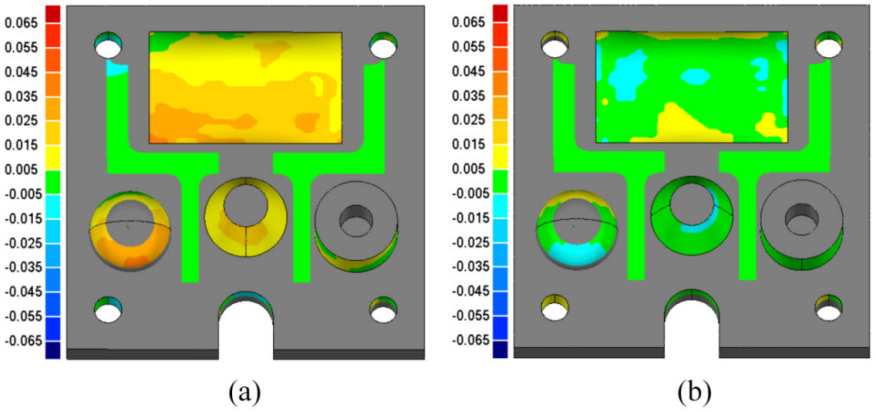

FIGURE 25. The comparison between probed points and reconstructed CAD model. (a) CAD model before compensation. (b) CAD model after data fusion.

constraint points of each section curve by equal chord deviation method. The positions of the constraint points on the curve with the most constraint points are used as the positions of the section planes for the X direction point cloud slicing. After the X direction data fusion, the obtained high precision section curves can then be used to compensate these section curves that are obtained by the previous Y direction slicing to obtain more high-precision section curves.

C. EXAMPLE THREE

Part C is a complex workpiece that contains both typical geometric features and free-form characteristics. The points measured by the laser scanner and tactile probe are shown in Fig. 24b, c, respectively. After data segmentation and fusion, a CAD model was reconstructed in the SolidWorks 2016 environment as shown in Fig. 24d.

1) MEASUREMENT SPEED COMPARISON FOR SENSORS

Table. 4 lists the numbers of raw measurement data points and measurement time. In the process of measuring part C, the time of laser scanning is 8 min 36 s and the time of tactile probing is 22 min 48 s, therefore the total measuring time is 31 min 24 s.

Finally, 278,654 laser scanning points are retained after data reduction to generate a satisfactory mesh surface for CAD model reconstruction, and 732 points measured from tactile probe are exploited to compensate the laser scanning data.

In comparison, if we assume that the measuring speed of the tactile probe is 1 point per second, based on the probing speed presented in Table. 4, it would take at least 77 hours to digitize the part using only a tactile method. The integration of the laser scanner and tactile probe, therefore, leads to much faster measurement than the tactile method alone.

2) CAD MODEL ACCURACY COMPARISON

To validate the quality of the final reconstructed CAD model, both uncompensated and compensated models are compared with data measured by CMM which can be regarded as the reference points on the actual surface. Fig. 25 presents the comparison between probed points and final reconstructed CAD models before and after compensation. We can see that the accuracy of the geometric elements of reconstructed CAD model has been greatly improved after data fusion.

TABLE 4. Numbers of points and measuring time.

Methods	Number of points	Measuring time (s)
Laser scanning	498,362	8:36
Tactile probe	732	22:48

VII. CONCLUSION

In this paper, an effective multi-sensor approach for the efficient and precise reverse engineering of complex geometry has been presented. Other existing multi-sensor configuration approaches only use optical sensors to capture the global surface information of the object and then guide the slower tactile probe to digitize the surface. The presented method is implemented through the incorporation of a laser line scanner and a tactile probe. The proposed system is unique in that it includes not only the physical integration of the two sensors but also their combination at the measurement information level. The laser scanner is used to digitize the overall object surface. Then the obtained geometric information is used to guide the tactile probe to re-measure the surface with a small number of sampling points. Finally, these high precision contact measurement data points are used to compensate non-contact measurement data to obtain a large number of high-precision measurement data for CAD model reconstruction. The results of the three case-study experiments show that the proposed approach offers an ideal compromise between precision and efficiency. A fast and precise measurement of complex geometry can be achieved. It has potential applications in a whole spectrum of manufacturing problems with a major impact on metrology, inspection, and reverse engineering.

To realize the high integration of reverse engineering, the integrated measurement system proposed in this paper is based on a CNC machine tool. The proposed measurement system has potential for improved accuracy if integrated into the CMM, which has higher kinematic accuracy than CNC machine tool.

The proposed curve deformation method is a global modification method. Local distortions of contour curves that are caused by the random error of non-contact measurement cannot be completely corrected. As shown in Fig. 21a, there are still some discretely distributed areas with relatively large measurement errors. Future work will focus on two aspects: on the one hand, we will work to reduce the uncertainty of non-contact measurement, so that the initial section contour curves can better grasp the geometric features of the measured surface, on the other hand, we will explore new method for multi-sensor measurement data fusion, such as multi-sensor information fusion technology based on evidence theory [40], [41].

ACKNOWLEDGMENT

The authors are grateful to all the reviewers for their valuable comments.

REFERENCES

[1] M. Sokovic and J. Kopac, "RE (reverse engineering) as necessary phase by rapid product development," *J. Mater. Process. Technol.*, vol. 175, nos. 1–3, pp. 398–403, Jun. 2006. doi: 10.1016/j.jmatprotec.2005.04.047.

[2] X. Ye, H. Liu, L. Chen, Z. Chen, X. Pan, and S. Zhang, "Reverse innovative design—An integrated product design methodology," *Comput.-Aided Des.*, vol. 40, no. 7, pp. 812–827, Jul. 2008. doi: 10.1016/j.cad.2007.07.006.

[3] S.-W. Hsiao and J.-C. Chuang, "A reverse engineering based approach for product form design," *Design Stud.*, vol. 24, no. 2, pp. 155–171, Mar. 2003. doi: 10.1016/s0142-694x(02)00030-3.

[4] Y. Wang and H.-Y. Feng, "Modeling outlier formation in scanning reflective surfaces using a laser stripe scanner," *Measurement*, vol. 57, pp. 108–121, Nov. 2014. doi: 10.1016/j.measurement.2014.08.010.

[5] M. Mahmud, D. Joannic, M. Roy, A. Isheil, and J.-F. Fontaine, "3D part inspection path planning of a laser scanner with control on the uncertainty," *Comput. Aided Des.*, vol. 43, no. 4, pp. 345–355, Apr. 2011. doi: 10.1016/j.cad.2010.12.014.

[6] Q. Tian, Y. Yang, X. Zhang, and B. Ge, "An experimental evaluation method for the performance of a laser line scanning system with multiple sensors," *Opt. Lasers Eng.*, vol. 52, pp. 241–249, Jan. 2011. doi: 10.1016/j.optlaseng.2013.06.002.

[7] S. Zhang, "Recent progresses on real-time 3D shape measurement using digital fringe projection techniques," *Opt. Lasers Eng.*, vol. 48, no. 2, pp. 149–158, Feb. 2010. doi: 10.1016/j.optlaseng.2009.03.008.

[8] U. V. Andersen, D. B. Pedersen, H. N. Hansen, and J. S. Nielsen, "In-process 3D geometry reconstruction of objects produced by direct light projection," *Int. J. Adv. Manuf. Technol.*, vol. 68, nos. 1–4, pp. 565–573, Sep. 2013. doi: 10.1007/s00170-013-4778-3.

[9] W. Lohry and S. Zhang, "3D shape measurement with 2D area modulated binary patterns," *Opt. Lasers Eng.*, vol. 50, no. 7, pp. 917–921, Jul. 2012. doi: 10.1016/j.optlaseng.2012.03.002.

[10] W. Yu and B. Xu, "A portable stereo vision system for whole body surface imaging," *Image Vis. Comput.*, vol. 28, no. 4, pp. 605–613, Apr. 2010. doi: 10.1016/j.imavis.2009.09.015.

[11] T. Pinto, C. Kohler, and A. Albertazzi, "Regular mesh measurement of large free form surfaces using stereo vision and fringe projection," *Opt. Lasers Eng.*, vol. 50, no. 7, pp. 910–916, Jul. 2012. doi: 10.1016/j.optlaseng.2012.03.003.

[12] A. Weckenmann, X. Jiang, K. D. Sommer, U. Neuschaefer-Rube, J. Seewig, L. Shaw, and T. Estler, "Multisensor data fusion in dimensional metrology," *CIRP Ann.*, vol. 58, no. 2, pp. 701–721, 2009. doi: 10.1016/j.cirp.2009.09.008.

[13] V. H. Chan, C. Bradley, and G. W. Vickers, "A multi-sensor approach for rapid digitization and data segmentation in reverse engineering," *J. Manuf. Sci. Eng.*, vol. 122, no. 4, pp. 725–733, Nov. 2000. doi: 10.1115/1.1286125.

[14] V. Carbone, M. Carocci, E. Savio, L. De Chiffre, and G. Sansoni, "Combination of a vision system and a coordinate measuring machine for the reverse engineering of freeform surfaces," *Int. J. Adv. Manuf. Technol.*, vol. 17, no. 4, pp. 263–271, Jan. 2001. doi: 10.1007/s001700170179.

[15] J. Sładek, P. M. Błaszczyk, M. Kupiec, and R. Sitnik, "The hybrid contact–optical coordinate measuring system," *Measurement*, vol. 44, no. 3, pp. 503–510, Mar. 2011. doi: 10.1016/j.measurement.2010.11.013.

[16] J. Sładek, R. Sitnik, M. Kupiec, and P. Błaszczyk, "The new hybrid method for fast and precision measurement," in *Proc. 18th IMEKO World Congr. Metrol. Sustain. Develop.*, Rio de Janeiro, Brazil, 2006, pp. 134–138.

[17] K. Lu and W. Wang, "A multi-sensor approach for rapid and precise digitization of free-form surface in reverse engineering," *Int. J. Adv. Manuf. Technol.*, vol. 79, nos. 9–12, pp. 1983–1994, Aug. 2015. doi: 10.1007/s00170-015-6960-2.

[18] K. Lu, W. Wang, Y. Wei, Z. Chen, and Y. Wu, "An adaptive sampling approach for digitizing unknown free-form surfaces based on advanced path detecting," *Procedia Cirp*, vol. 10, pp. 216–223, 2013. doi: 10.1016/j.procir.2013.08.034.

[19] C. Bradley and V. Chan, "A complementary sensor approach to reverse engineering," *J. Manuf. Sci. Eng.*, vol. 123, no. 1, pp. 74–82, 2001. doi: 10.1115/1.1349556.

[20] X. Zexiao, J. Jianguo, and Z. Qiumei, "Complete 3D measurement in reverse engineering using a multi-probe system," *Int. J. Mach. Tools Manuf.*, vol. 45, nos. 12–13, pp. 1474–1486, Oct. 2005. doi: 10.1016/j.ijmachtools.2005.01.028.

[21] H. Zhao, J.-P. Kruth, N. Van Gestel, B. Boeckmans, and P. Bleys, "Automated dimensional inspection planning using the combination of laser scanner and tactile probe," *Measurement*, vol. 45, pp. 1057–1066, Jun. 2012. doi: 10.1016/j.measurement.2012.01.037.

[22] L. Mu, Z. Yin, and Y. Xiong, "A multisensor based on machine inspection approach for freeform surfaces," in *Proc. Int. Conf. Transp., Mech., Electr. Eng.*, Changchun, China, Dec. 2012, pp. 2166–2169.

[23] A, Mohib, A, Azab, and H. El-Maraghy, "Feature-based hybrid inspection planning: A mathematical programming approach," *Int. J. Comput. Integr. Manuf.*, vol. 22, no. 1, pp. 13–29, Jan. 2009. doi: 10.1080/09511920802382368.

[24] P. X. Liu, H.-L. Jia, and Z. Wei, "Data fusion for free-form surfaces in reverse engineering," in *Proc. 3th Int. Conf. Mater. Eng., Manuf. Technol. Control*, Taiyuan, China, Apr. 2016, pp. 1443–1448.

[25] Y. Huang and X. Qian, "A dynamic sensing-and-modeling approach to three-dimensional point- and area-sensor integration," *J. Manuf. Sci. Eng.*, vol. 129, pp. 623–635, Jun. 2007. doi: 10.1115/1.2714585.

[26] Y. Huang and X. Qian, "Dynamic *B*-spline surface reconstruction: Closing the sensing-and-modeling loop in 3D digitization," *Comput. Aided Des.*, vol. 39, pp. 987–1002, Nov. 2007. doi: 10.1016/j.cad.2007.06.008.

[27] F. Li, A. P. Longstaff, S. Fletcher, and A. Myers, "Rapid and accurate reverse engineering of geometry based on a multi-sensor system," *Int. J. Adv. Manuf. Technol.*, vol. 74, pp. 369–382, Sep. 2014. doi: 10.1007/s00170-014-5997-y.

[28] M. J. Ren, L. J. Sun, C. F. Cheung, Y. H. Yin, Y. L. Cao, and M. Y. Liu, "A weighted least square based data fusion method for precision measurement of freeform surfaces," *Precis. Eng.*, vol. 48, pp. 144–151, Apr. 2016. doi: 10.1016/j.precisioneng.2016.11.014.

[29] B. M. Colosimo, M. Pacella, and N. Senin, "Multisensor data fusion via Gaussian process models for dimensional and geometric verification," *Precis. Eng.*, vol. 40, pp. 199–213, Apr. 2015. doi: 10.1016/j.precisioneng.2014.11.011.

[30] M. B. Rak, A. Wozniak, and J. R. R. Mayer, "The use of low density high accuracy (LDHA) data for correction of high density low accuracy (HDLA) point cloud," *Opt. Lasers Eng.*, vol. 81, pp. 140–150, Jun. 2016. doi: 10.1016/j.optlaseng.2016.01.005.

[31] J. Tao and K. Jiyong, "A 3-D point sets registration method in reverse engineering," *Comput. Ind. Eng.*, vol. 53, no. 2, pp. 270–276, 2007. doi: 10.1016/j.cie.2007.06.020.

[32] M. Pauly, M. Gross, and L. P. Kobbelt, "Efficient simplification of point-sampled surfaces," in *Proc. IEEE Conf. Vis.*, Boston, MA, USA, Oct./Nov. 2002, pp. 70–163.

[33] J. Zhang, J. Cao, X. Liu, J. Wang, J. Liu, and X. Shi, "Point cloud normal estimation via low-rank subspace clustering," *Comput. Graph.*, vol. 37, no. 6, pp. 697–706, Oct. 2013. doi: 10.1016/j.cag.2013.05.008.
[34] X. Liu, J. Zhang, J. Cao, B. Li, and L. Liu, "Quality point cloud normal estimation by guided least squares representation," *Comput. Graph.*, vol. 51, pp. 106–116, Oct. 2015. doi: 10.1016/j.cag.2015.05.024.
[35] J. Cao, H. Chen, Y. Li, X. Liu, C. Zou, and J. Zhang, "Normal estimation via shifted neighborhood for point cloud," *J. Comput. Appl. Math.*, vol. 329, pp. 57–67, Feb. 2018. doi: 10.1016/j.cam.2017.04.027.
[36] M. Hubert, P. J. Rousseeuw, and K. V. Branden, "ROBPCA: A new approach to robust principal component analysis," *Technometrics*, vol. 47, no. 1, pp. 64–79, Feb. 2005. doi: 10.1198/004017004000000563.
[37] I. Assem and G. Dupont, "Friezes and a construction of the Euclidean cluster variables," *J. Pure Appl. Algebra*, vol. 215, no. 10, pp. 2322–2340, Oct. 2011. doi: 10.1016/j.jpaa.2010.12.013.
[38] Y. Wang, J. Wang, T. Chu, M. Liu, T. Yang, and X. Chen, "Feature surface extraction and reconstruction from industrial components using multistep segmentation and optimization," *Remote Sens.*, vol. 10, no. 7, p. 1073, 2018. doi: 10.3390/rs10071073.
[39] S. F. F. Gibson and B. Mirtich, "A survey of deformable modeling in computer graphics," Mitsubishi Electr. Res. Lab., Cambridge, MA, USA, Tech. Rep. TR-97-19, Nov. 1997.
[40] F. Xiao, "Multi-sensor data fusion based on the belief divergence measure of evidences and the belief entropy," *Inf. Fusion*, vol. 46, pp. 23–32, Mar. 2019. doi: 10.1016/j.inffus.2018.04.003.
[41] F. Xiao and B. Qin, "A weighted combination method for conflicting evidence in multi-sensor data fusion," *Sensors*, vol. 18, no. 5, p. 1487, 2018. doi: 10.3390/s18051487.

ZHIQIANG YU received the B.S. degree from Southwest University, Chongqing, China, in 2013. He is currently pursuing the Ph.D. degree with the School of Mechanical, Tianjin University, Tianjin, China. His research interests include optical measurement, reverse engineering, on-line measurement, and multisensor measurement data fusion.

TAIYONG WANG received the M.S. and Ph.D. degrees in mechanical engineering from Tianjin University, Tianjin, China, in 1986 and 1995, respectively.

He is currently a Professor with the School of Mechanical, Tianjin University, and the Chairman of the International Conference on Intelligent Manufacturing and Mechanical Dynamics (ICIMT&MD), the Executive Director of the Chinese Society for Measurement, the Chairman of the Mechanical Dynamics Society of Chinese Society for Vibration Engineering, and the Vice Chairman of the Mechanical Fault Diagnosis Society of Chinese Society for Vibration Engineering. He has authored or coauthored more than 200 influential articles and technical articles. His research interests include intelligent fault diagnosis and maintenance, intelligent manufacturing systems, and reconfigurable CNC systems. He was a recipient of the Second Prize of the National Science and Technology Progress Award.

PENG WANG (M'19) received the B.S. degree from the Huazhong University of Science and Technology, Wuhan, China, in 2010, and the Ph.D. degree in mechanical engineering from Tianjin University, Tianjin, China, in 2018. He is currently an Assistant Professor with the School of Mechanical, Tianjin University. His research interests include time–frequency signal processing method, intelligent mechanical fault diagnosis, and development of intelligent diagnosis instruments.

YING TIAN received the M.S. and Ph.D. degrees in mechanical engineering from the Harbin Institute of Technology (HIT), Heilongjiang, China, in 2003, and the Ph.D. degree in mechanical engineering from Tianjin University, Tianjin, China, in 2010. She is currently an Associate Professor with the School of Mechanical, Tianjin University, and the Executive Vice Secretary-General of the Production Engineering Branch of the Chinese Society of Mechanical Engineering–Committee of Machine tool. Her research interests include methodology of dynamic energy efficiency modeling for intelligent equipment systems, health condition monitoring and intelligent maintenance based on energy efficiency index, and high energy efficiency green manufacturing process and equipment.

HONGBIN LI received the B.S. degree from the Wuhan University of Technology, Wuhan, China, in 2013. He is currently pursuing the Ph.D. degree with the School of Mechanical, Tianjin University, Tianjin, China. His research interests include fused deposition modeling, selective laser melting, the mechanical property of FDM part and SLM part, and interface mechanics.